Potential energy surface and rate coefficients of protonated cyanogen (HNCCN+) induced by collision with helium (He) at low temperature

Cheikh Bop, N. P. Faye, K. Hammami

Monthly Notices
of the
ROYAL ASTRONOMICAL SOCIETY

MNRAS **478,** 4410–4415 (2018)
Advance Access publication 2018 May 25

doi:10.1093/mnras/sty1385

Potential energy surface and rate coefficients of protonated cyanogen ($HNCCN^+$) induced by collision with helium (He) at low temperature

Cheikh T. Bop,[1]★ N. A. B. Faye[1] and K. Hammami[2]

[1]*Laboratory of Atoms Lasers, Department of Physics, Faculty of Science and Technique, University Cheikh Anta Diop of Dakar, Dakar 5005, Senegal*
[2]*Laboratory of Atomic Molecular Spectroscopy and Applications, Department of Physics, Faculty of Sciences, University Tunis El Manar, Campus Universities, 1060 Tunis, Tunisia*

Accepted 2018 May 18. Received 2018 May 18; in original form 2018 April 14

ABSTRACT

Nitriles have been identified in space. Accurately modelling their abundance requires calculations of collisional rate coefficients. These data are obtained by first computing potential energy surfaces (PES) and cross-sections using high accurate quantum methods. In this paper, we report the first interaction potential of the $HNCCN^+$–He collisional system along with downward rate coefficients among the 11 lowest rotational levels of $HNCCN^+$. The PES was calculated using the explicitly correlated coupled cluster approach with simple, second, and non-iterative triple excitation (CCSD(T)–F12) in conjunction with the augmented-correlation consistent-polarized valence triple zeta Gaussian basis set. It presents two local minima of $\sim$283 and $\sim$136 cm^{-1}, the deeper one is located at $R = 9\ a_0$ towards the H end ($He\cdots HNCCN^+$). Using the so-computed PES, we calculated rotational cross-sections of $HNCCN^+$ induced by collision with He for energies ranging up to 500 cm^{-1} with the exact quantum mechanical close coupling method. Downward rate coefficients were then worked out by thermally averaging the cross-sections at low temperature ($T \leq 100$ K). The discussion on propensity rules showed that the odd Δj transitions were favoured. The results obtained in this work may be crucially needed to accurately model the abundance of cyanogen and its protonated form in space.

Key words: molecular data – molecular processes – ISM: abundances – ISM: molecules.

1 INTRODUCTION

The chemistry of nitriles (R–C≡N) is astronomically crucial due to their abundance in the interstellar medium. In fact, cyanopolyynes ($HC_{2n+1}N$) are ubiquitous in interstellar and circumstellar clouds as TMC-1 and IRC+10216 (Bell et al. 1997; Balucani et al. 2000; Chin et al. 2006). Petrie, Millar & Markwick (2003) and Kołos & Grabowski (2000) have proposed that dicyanopolyynes (N≡C–$(C\equiv C)_n$–C≡N) would also be present in these regions. This hypothesis may have a great impact on the abundance of the interstellar CN radical (Rodriguez-Franco, Martin-Pintado & Fuente 1998; Fray et al. 2005; Riechers et al. 2007). Indeed, the CN radical observed in the cometary comae is expected to be the main product of cyanogen (NCCN) dissociation (Wu & Hall 1994; North & Hall 1997).

NCCN was detected towards the atmosphere of Titan (Kunde et al. 1981; Coustenis et al. 1991) with Voyager 1 through infrared observations. Due to their lack of permanent electric dipole moment, the dicyanopolyynes are not observable in radio astronomy. Therefore, to prove the NCCN abundance:

(i) one of the suggested possibilities is to rely on the analogue P-bearing molecule, namely NCCP, which has a permanent electric dipole moment of 6.347 (Puzzarini & Cazzoli 2009). It is worth mentioning that Agúndez, Cernicharo & Guélin (2014) reported a column density of 7×10^{11} cm^{-2} as well as a tentative of identification towards the IRC+10216 with the IRAM 30 m telescope for NCCP;

(ii) an alternative pathway is to probe the polar isomer NCNC that is metastable or the protonated form, namely protonated cyanogen ($HNCCN^+$) (Petrie et al. 2003). This was later detected towards the TMC-1 and L483 cold dark clouds showing the $5 \longrightarrow 4$ and $10 \longrightarrow 9$ rotational emission lines at 44 GHz using the Yebes 40 m telescope and at 88.8 GHz with the IRAM 30 m telescope, respectively (Agúndez et al. 2015).

Furthermore, protonation processes are very current in space and planetary atmosphere mainly for nitriles. In the atmosphere of Titan where cyanogen was already detected, Coustenis et al. (1991), Kunde et al. (1981), and Anicich & McEwan (1997) have suggested the following mechanisms of formation (equations 1 and 2) for the protonated cyanogen.

$$H_3^+ + NCCN \longrightarrow HNCCN^+ + H_2 \quad (1)$$

★ E-mail: aacatbop@gmail.com

$$C_2H_3^+ + NCCN \longrightarrow HNCCN^+ + C_2H_2 \quad (2)$$

$$HCO^+ + NCCN \longrightarrow HNCCN^+ + CO \quad (3)$$

The presence of the H_3^+ reactant in the TMC-1 and L483 cold dark clouds with relatively large abundances, supplemented by the relatively large proton affinity (PA) of NCCN [PA(NCCN) $\approx$651.2 kJ mol^{-1} (Milligan & Fairley 1998) which is greater than PA(H_2) $\approx$ 422.3 kJ mol^{-1} (Hunter & Lias 1998)], makes equation (1) the most promising channel for the production of the interstellar HNCCN$^+$. In addition, the reaction of proton transfer (equation 3) has been proposed by Agúndez et al. (2015). Along with HNCCN$^+$ (Agúndez et al. 2015), some protonated nitriles HCNH$^+$, HC3NH$^+$ (Ziurys, Apponi & Yoder 1992; Kawaguchi et al. 1994) and numerous other protonated molecules have been detected towards cold media. This suggests that protonated molecules play a crucial role in the chemistry of cold astronomical sources.

Cationic nitriles have been the target of numerous theoretical as well as experimental investigations (Cazzoli, Degli Esposti & Scappini 1992; Botschwina, Fluegge & Seeger 1993; Gottlieb et al. 2000; Ding et al. 2001; Semaniak et al. 2001; Amano, Hashimoto & Hirao 2006; McLain & Adams 2009; Puzzarini & Cazzoli 2009). Most of them were focused on the study of the protonated nitriles destruction through dissociative recombination. However, radiative transitions as well as collisional rate coefficients are crucially needed to accurately model their abundance in the interstellar molecular clouds (Roueff & Lique 2013). Without these data, one would assume the physical conditions of local thermodynamic equilibrium, which are rarely reached in space. As far as we know, the only relevant astrophysical investigation focused on the collisional processes for a protonated nitrile (HCNH$^+$) is that of Nkem et al. (2014).

In this paper, we focused on the investigation of dynamical processes of protonated cyanogen induced by collision with helium (He) at low temperature. Using He as collision partner is a relevant choice as one can derive the rate coefficients that would be obtained with para-H_2 ($j = 0$) as projectile. In fact, He may be a suitable template for para-H_2 as it is a closed shell atom that contains two electrons. However, the accuracy of such an approximation is discussed in the literature for protonated species. Nevertheless, it roughly yields to the scattering data that would be recorded from protonated molecule-para-H_2 in terms of magnitude rank. In the case of long-chain molecules, Wernli et al. (2007) showed that the use of the 1.4 scaling mass factor is a good approximation. It is worth noting that the interactions between protonated molecules and H_2 generally lead to deep potential wells towards the H end. Such strong attractions along with low rotational constants (in the case of nitriles with long chain) make the dynamical processes computationally expensive. Such a difficulty may be an additional reason to the use of He instead of H_2 as collision partner (Daniel et al. 2005; Dubernet, Quintas-Sánchez & Tuckey 2015; Bop et al. 2017b; Werfelli et al. 2017). According to the physical conditions of the media where HNCCN$^+$ was observed (TMC-1 and L483 cold clouds), the rate coefficients calculations were carried out at low temperature. High accurate quantum mechanical calculations based on a reliable ab initio potential were used to satisfy the required astrophysical precision.

This paper is structured as follows: Section 2 presents the interaction potential. The scattering calculations are described and discussed in Section 3. In Section 4, are given concluding remarks.

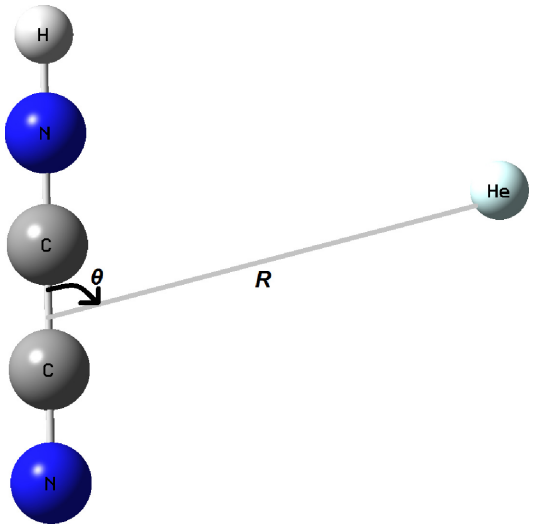

Figure 1. Description of the body-fixed Jacobi coordinate system.

2 POTENTIAL ENERGY SURFACE AND ANALYTICAL FIT

The potential energy surface (PES) constructed in this work results from the interactions between a linear molecule and a structureless atom. To keep the number of degrees of freedom reasonably small, the rigid rotor approximation can be safely used in the calculations. Previous investigations (Jeziorska et al. 2000; Jankowski & Szalewicz 2005) have suggested that averaged geometries (r_0 geometries) lead to a better description of PES than equilibrium molecular geometries (r_e geometries). The r_0 geometries can be computed using ground state vibrational wave functions. To the best of our knowledge, such eigenstates are not available in the literature for protonated cyanogen. Therefore, we relied on the experimental equilibrium geometries of Cazzoli et al. (1992) which were derived from the rotational constants of HNCCN$^+$($X^1\Sigma^+$) and its isotopes. Typically, the resulting bond lengths are $r_{HN_1} = 1.0057$ Å, $r_{N_1C_1} = 1.140$ Å, $r_{C_1C_2} = 1.376$ Å, and $r_{C_2N_2} = 1.158$ Å. These values should be in good agreement with the vibrationally averaged ones.

The HNCCN$^+$–He collisional complex was described with the body-fixed Jacobi coordinates system θ and $\boldsymbol{R}$, where $\boldsymbol{R}$ represents the vector between the centre of masses of the two collision partners and θ stands for the angle between the vector $\boldsymbol{R}$ and the HNCCN$^+$ rod. From Fig. 1, one can see that $\theta = 0^\circ$ corresponds to the He approach towards the H end. Hereafter, the potential was constructed with 1064 ab initio points that were treated in the Cs symmetry group. The radial coordinate ($R = |\boldsymbol{R}|$) was varied from 4 to 30 a_0 using an irregular grid. For $4 \leq R \leq 15$ the grid was set to 0.25 a_0, for $15 \leq R \leq 20$ to 1 a_0 and for $20 \leq R \leq 30$ to 2 a_0. In addition, $R = 100$ a_0 was included for reasons we will explicit in the next paragraph. The scattering angle θ was uniformly spanned from 0 to 180° with a step of 10°.

To compute the HNCCN$^+$($X^1\Sigma^+$)–He(^1S) van der Waals interaction potential, preliminary calculations were performed with the complete active space self-consistent field method (Knowles & Werner 1985; Werner & Knowles 1985) to weigh out the monoconfigurational character of the collisional system over the 1064 ab initio points mentioned above. The static weight of the predominant configuration of the HNCCN$^+$–He ground electronic state is greater than 93 per cent. Then, we used the explicitly correlated coupled

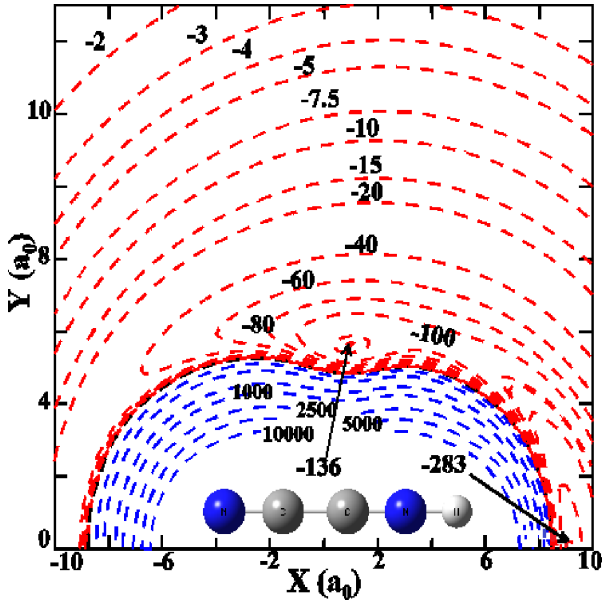

Figure 2. Contour plots of the $HNCCN^+$–He potential energy surface (in unit of cm^{-1}) as a function of x and y $x = R\cos(\theta)$ and $y = R\sin(\theta)$). The $HNCCN^+$ molecule is shown to scale.

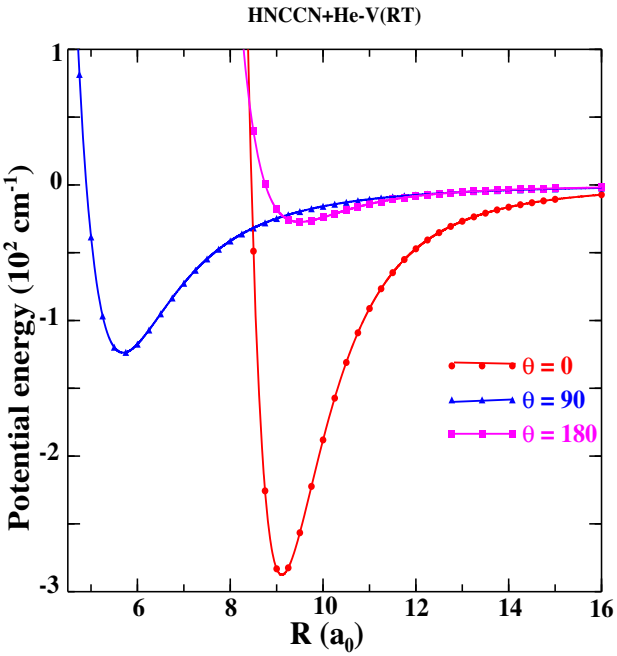

Figure 3. Potential energy surface (in unit of cm^{-1}) of the $HNCCN^+$–He for selected geometries ($\theta = 0$, 90, and 180°).

cluster approach with single, double, and non-iterative triple excitation CCSD(T)-F12 (Knizia, Adler & Werner 2009) to calculate the PES adopting the same methodology we followed in our previous papers (Bop et al. 2017a,b). The atoms of the collisional system were described using the augmented-correlation consistent-polarized valence triple zeta (aug-cc-pVTZ) basis set. Both of the method and the basis set (i.e. the level of theory, hereafter denoted as CCSD(T)-F12/aug-cc-pVTZ) were used as implemented in the MOLPRO molecular package (version 2010) (Werner et al. 2010). The counterpoise procedure of Boys & Bernardi (1970) was used to correct the errors generated by the basis set superposition (see equation 4). In addition, the size consistency error was corrected by subtracting to the global potential the energy value (which is close to 5.7 cm^{-1} for all He orientations) calculated at $R = 100\,a_0$. Hence, the interaction potential is constrained to asymptotically decay to zero.

$$V(R,\theta) = E_{HNCCN^+-He}(R,\theta) - E_{HNCCN^+}(R,\theta) - E_{He}(R,\theta). \quad (4)$$

Although the accuracy of the CCSD(T)-F12/aug-cc-pVTZ level of theory has been approved in the literature, it was checked in our previous works (Bop et al. 2017b; Bop, Hammami & Faye 2017c).

We present in Fig. 2 equipotential of the $HNCCN^+$–He van der Waals system. The contours show a prolate ellipsoid symmetry due to the dominance of the rod-like shape of $HNCCN^+$. The red contours represent the negative potentials (attractive part) while the blue contours stand for the positive potentials (the repulsive part). This interaction potential presents two local minima. The shallower one, 136.24 cm^{-1}, is observed at $\{R = 5.75\,a_0, \theta = 80.0°\}$ i.e. $\{x = 1.00\,a_0, y = 5.66\,a_0\}$. The deeper potential well (283.11 cm^{-1}) is located at $\{R = 9.00\,a_0, \theta = 0.0°\}$ i.e. $\{x = 9.00\,a_0, y = 0.00\,a_0\}$ towards the H end of the $HNCCN^+$ rod. As illustrated in Fig. 3, the interaction potential presents a strong anisotropy. The potential well varies steadily from one orientation to another. Typically the well depth is 283.11 cm^{-1} for $\theta = 0°$, 123.48 cm^{-1} for $\theta = 90°$, and 27.28 cm^{-1} for $\theta = 180°$.

In order to solve the coupled equations for the scattering study, expanding the PES over a basis of suitable angular functions for each R-distance is needed. In general, the Legendre polynomial functions are used (see equation 5) for the atom-rigid linear rotor collisional systems (V_λ and P_λ represent the radial coefficients and the angular functions, respectively). However, when using equation (5) to expand the HC_3N–He potential, Green & Chapman (1978) noticed convergence problems.

$$V(R,\theta) = \sum_{\lambda=0}^{\lambda_{max}} V_\lambda(R) P_\lambda(\cos\theta). \quad (5)$$

Then, they performed quasi-classical trajectory calculations instead of quantum computations. This convergence failure is due to the fact that the spherical symmetry of molecules decreases with the length of their chain. To overcome such a problem, it is necessary to include in the expansion (equation 5) a large number of radial coefficients. Indeed, Wernli et al. (2007) used $\lambda_{max} = 35$ to fit the HC_3N–He regularized potential within an error of a few cm^{-1}. In this work, the same number of radial coefficients was used to expand the PES over the basis of Legendre polynomial functions. Although we did not regularize the PES, the 35 anisotropic terms have generated an analytical PES similar to the ab initio one. Deviations are observed only for the T-shape geometry at $R = 5\,a_0$ (see the supplementary file to appreciate the accuracy of the PES expansion). We expect that this slight discrepancy will not affect significantly the dynamic results.

According to Fig. 4, which depicts the expansion of the $V_{\lambda=0-3}$ radial coefficients as a function of R, V_1 is the largest in magnitude among the anisotropic terms (terms for which $\lambda > 0$). The dominance of such a term may have a consequence on the behaviour of the dynamic results.

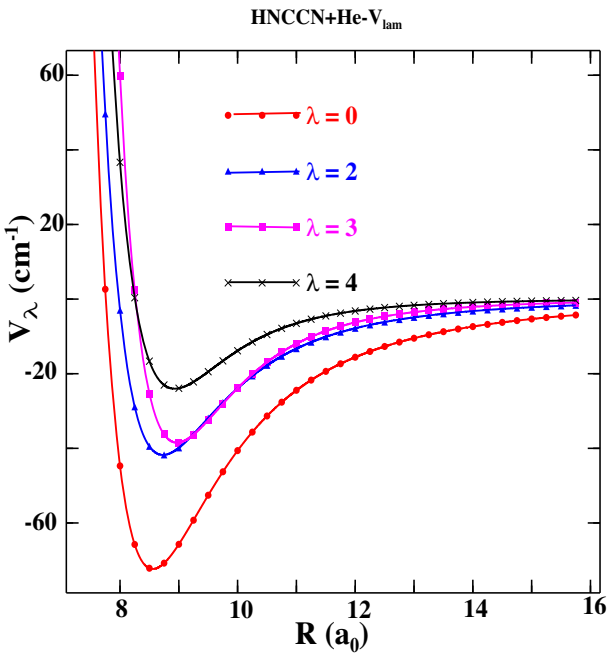

Figure 4. Comparison of the anisotropic radial coefficients $V_{\lambda=1-3}$ with respect to the isotropic term $V_{\lambda=0}$.

3 DYNAMIC STUDY

As we focused on low-temperature rotational rate coefficients, the total energy (E) range was spanned up to 500 cm^{-1}. For the HNCCN$^+$ molecule, this maximum energy is low enough to consider the transitions purely rotational.

3.1 Cross-sections

The rotational inelastic cross-sections presented in this paper were computed using the close coupling (CC) approach, developed by Arthurs & Dalgarno (1960), as it is implemented in the MOLSCAT code (Hutson & Green 1994). During the scattering computations, the log derivative propagator of Manolopoulos (1986) was used to solve the coupled equations. For this purpose, preliminary calculations were carried out as convergence tests to fix the propagator parameters. The integration boundaries were set to $R_{\rm min} = 3\ a_0$ and $R_{\rm max} = 90\ a_0$. The STEPS parameter was set large enough at low energy, to generate a fine integration grid, as it is inversely proportional to the integration step. Typically, STEPS = 30 for $E \leq 50\,{\rm cm}^{-1}$ and 10 for the other energy values. Due to the large value of $\lambda_{\rm max}$ used in the expansion, equation (5), the rotational basis was set large enough to include all coupling coefficients (V_λ) in the dynamic calculations. Therefore, all opened channels along with a large number of closed channels were taken into account. This led to high accurate scattering data that were computationally expensive. For instance, $j_{\rm max}$ was set to 20 for $E \leq 25\,{\rm cm}^{-1}$, and progressively increased up to $j_{\rm max} = 30$ for a total energy of 500 cm^{-1}. These $j_{\rm max}$ values were determined by optimizing the rotational basis. All parameters of the propagator are listed in Table 1 along with the spectroscopic constants, namely B_e and D_e as well as the reduced mass μ of the collisional system. The total energy range 0.3–300 cm^{-1} was spanned as follows: for $E \leq 30\,{\rm cm}^{-1}$ the step was set to 0.1 cm^{-1}, for $30 \leq E \leq 50\,{\rm cm}^{-1}$ to 0.5 cm^{-1}, for $50 \leq E \leq 100\,{\rm cm}^{-1}$ to 1 cm^{-1}, for $100 \leq E \leq 200\,{\rm cm}^{-1}$ to 5 cm^{-1}, for $200 \leq E \leq 300\,{\rm cm}^{-1}$ to 10 cm^{-1}, and for $300 \leq E \leq 500\,{\rm cm}^{-1}$ to 20 cm^{-1}.

Table 1. Parameters of the propagator used in this work.

$B_e = 0.148\,{\rm cm}^{-1}$, [a]	$j_{\rm max} = 20, 22, 25, 27, 30$
$D_e = 0.177 \times 10^{-6}\,{\rm cm}^{-1}$, [a]	STEPS = 30, 10
$\mu = 3.71$ au	$R_{\rm min}, R_{\rm max} = 3, 90\ a_0$

[a] Stands for Cazzoli et al. (1992).

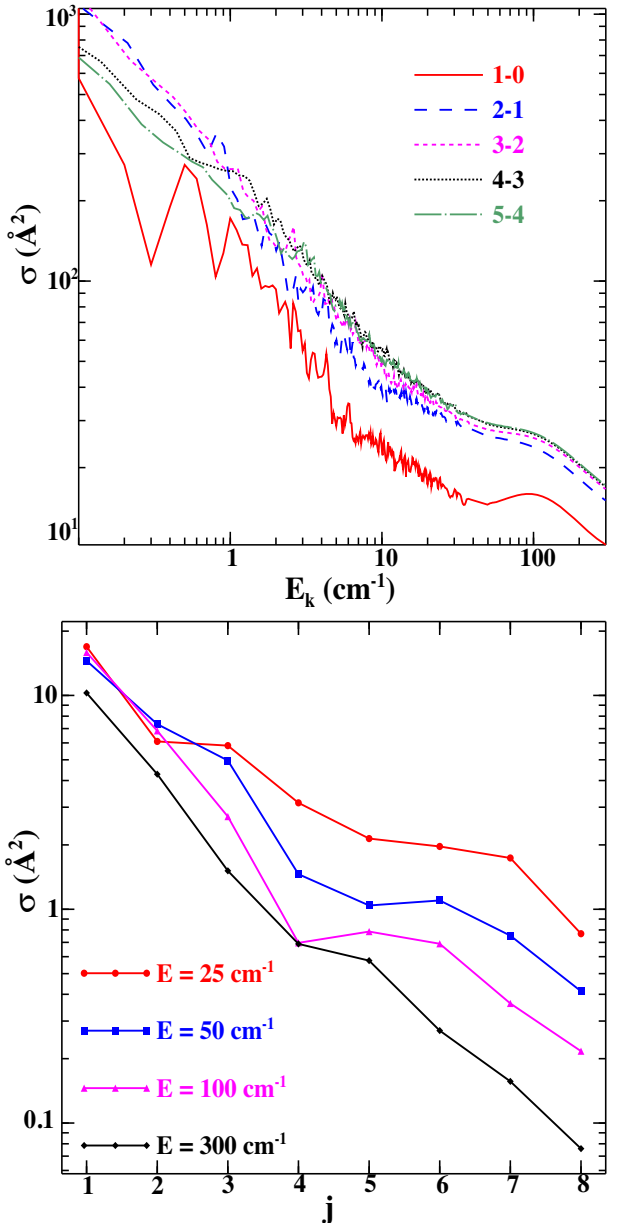

Figure 5. Inelastic cross-sections ($\sigma_{j+1\longrightarrow j}$, upper panel and $\sigma_{j\longrightarrow 0}$, lower panel) of HNCCN$^+$ due to He impact: as a function of the kinetic energy ($E_{\rm k}$) (upper panel) and as a function of the initial rotational level (j) for selected energies (lower panel).

We depict in Fig. 5 rotational de-excitation cross-sections of protonated cyanogen due to collision with helium. The upper panel shows several resonances for kinetic energies below 30 cm^{-1}. It is noteworthy that the small energy step used in the calculations of cross-sections has yielded the correct description of these

resonances (shape and Feshbach). The Feshbach resonances occur when the projectile (helium) is trapped in the potential well leading to temporary quasi-bound states of the $HNCCN^+$–He collisional system. The shape resonances may be explained as quasi-bound states due tunnelling through the centrifugal energy barrier. Concerning propensity rules, we rely on the lower panel of Fig. 5 since the $3 \longrightarrow 2$, $4 \longrightarrow 3$, and $5 \longrightarrow 4$ transitions overlap (for $E_k \geq 2\,cm^{-1}$). This panel shows that, for all selected energies, the odd j values (1, 3, 5, and 7) outweigh the even ones (2, 4, 6, and 8, respectively). As expected from the behaviour of radial coefficients (see Fig. 4), the odd Δj transitions are favoured.

3.2 Rate coefficients

By thermally averaging the so-computed cross-sections with the Maxwell–Boltzmann velocity distribution, we worked out the rotational collision rates for kinetic temperatures (T) ranging from 1 to 100 K.

$$k_{j\longrightarrow j'}(T) = \left(\frac{8}{\pi\mu\beta}\right)^{1/2} \beta^2 \int_0^\infty E_k \sigma(E_k) e^{-\beta E_k} dE_k, \quad (6)$$

$\beta = 1/k_B T$ while k_B stands for the constant of Boltzmann. The kinetic energy E_k is derived from the total energy, $E_k = E - E_j$, where the rotational energy $E_j = B_e j(j+1) - D_e j^2(j+1)^2$. The downward collision rates were carried out for rotational transitions involving the 11 first levels.

The upper panel of Fig. 6 shows the variation of rate coefficients as a function of the kinetic temperature. All transitions present the same shape. The magnitude of rate coefficients increases when j increases. This pattern is observed in the entire temperature range for the three lowest transitions while it appears only at $T \geq 40$ K for the higher transitions. Although the $5 \longrightarrow 4$ rotational transition predominates the $4 \longrightarrow 3$ one, their magnitudes are quite comparable. These similarities persist for the $(j = 6\text{–}10) \longrightarrow (j-1)$ transitions (see supplementary materials). Therefore, both items (the pattern and the similar magnitudes discussed above) together show that the $(j = 4\text{–}10) \longrightarrow (j-1)$ rotational transitions are dominant and they almost overlap.

In order to discuss propensity rules, we depict in the lower panel of Fig. 6 downward rate coefficients ($k_{j\longrightarrow 0}$) as a function of the initial rotation level j. As expected from the behaviour of cross-sections, the odd Δj transitions are favoured.

4 CONCLUSION

Rotational inelastic cross-sections of protonated cyanogen due to helium impact have been determined using the exact CC quantum mechanical method for energies ranging up to 500 cm^{-1}. These data were then thermally averaged using the Maxwell–Boltzmann velocity distribution to calculate downward rate coefficients among the 11 lowest rotational levels for kinetic temperatures ranging from 1 to 100 K. These dynamic calculations were based on a high accurate ab initio PES. This latter was computed using the explicitly correlated coupled cluster approach with single, double, and non-iterative triple excitation in conjunction with the aug-cc-pVTZ Gaussian basis set.

Concerning propensity rules, the transitions involving odd Δj values are favoured for cross-sections as well as for rate coefficients. These later showed that the $(j = 4\text{–}10) \longrightarrow (j-1)$ transitions predominate from 40 to 100 K.

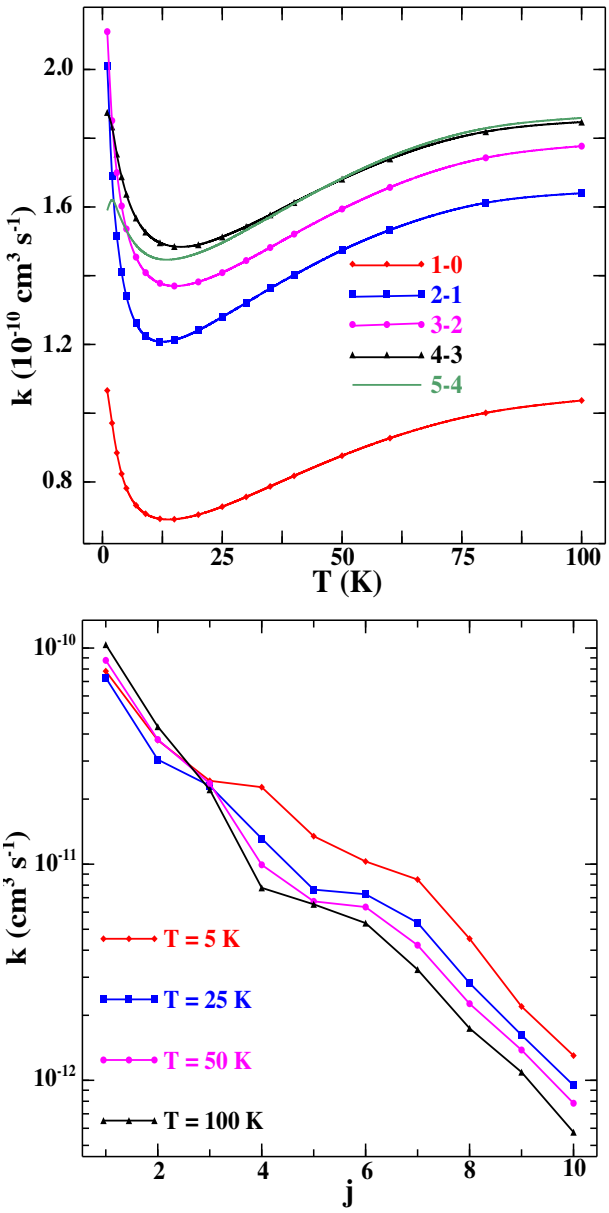

Figure 6. Downward rate coefficients (k) of $HNCCN^+$ due to He impact as a function of the kinetic temperature for $j+1 \longrightarrow j$ ($j = 0\text{–}4$, upper panel) and $j \longrightarrow 0$ ($j = 1\text{–}10$, lower panel) transitions.

The data presented in this paper may be of great astrophysical interest in the accurate modelling of cyanogen and protonated cyanogen abundances in space.

ACKNOWLEDGEMENTS

The authors warmly acknowledge many conversations with the Pr. Alexandre Faure of the Institut de Planétologie et d'Astrophysique de Grenoble, Université Grenoble Alpes, 414 Rue de la Piscine, Grenoble CEDEX 9, France.

REFERENCES

Agúndez M., Cernicharo J., Guélin M., 2014, A&A, 570, A45
Agúndez M. et al., 2015, A&A, 579, L10

Amano T., Hashimoto K., Hirao T., 2006, J. Mol. Struct., 795, 190
Anicich V. G., McEwan M. J., 1997, Planet. Space Sci., 45, 897
Arthurs A., Dalgarno A., 1960, Proc. R. Soc. A, 256, 540
Balucani N., Asvany O., Huang L., Lee Y., Kaiser R., Osamura Y., Bettinger H., 2000, ApJ, 545, 892
Bell M., Feldman P., Travers M., McCarthy M., Gottlieb C., Thaddeus P., 1997, ApJ, 483, L61
Bop C. T., Boye Faye N., Hammami K., Jaïdane N., 2017a, J. Phys. Chem. A, 121, 7854
Bop C. T., Hammami K., Niane A., Faye N., Jaïdane N., 2017b, MNRAS, 465, 1137
Bop C. T., Hammami K., Faye N., 2017c, MNRAS, 470, 2911
Botschwina P., Fluegge J., Seeger S., 1993, J. Mol. Spectrosc., 157, 494
Boys S. F., Bernardi F. d., 1970, Mol. Phys., 19, 553
Cazzoli G., Degli Esposti C., Scappini F., 1992, J. Chem. Phys., 97, 6187
Chin Y.-n., Kaiser R. I., Lemme C., Henkel C., 2006, AIP Conf. Proc. Vol. 855, Detection of Interstellar Cyanoallene and its Implications for Astrochemistry. Am. Inst. Phys., Milville, NY, p. 149
Coustenis A., Bezard B., Gautier D., Marten A., Samuelson R., 1991, Icarus, 89, 152
Daniel F., Dubernet M.-L., Meuwly M., Cernicharo J., Pagani L., 2005, MNRAS, 363, 1083
Ding Y.-H., Li Z.-S., Huang X.-R., Sun C.-C., 2001, J. Phys. Chem. A, 105, 7085
Dubernet M.-L., Quintas-Sánchez E., Tuckey P., 2015, J. Chem. Phys., 143, 044315
Fray N., Bénilan Y., Cottin H., Gazeau M.-C., Crovisier J., 2005, Planet. Space Sci., 53, 1243
Gottlieb C., Apponi A., McCarthy M., Thaddeus P., Linnartz H., 2000, J. Chem. Phys., 113, 1910
Green S., Chapman S., 1978, ApJS, 37, 169
Hunter E. P., Lias S. G., 1998, J. Phys. Chem. Ref. Data, 27, 413
Hutson J. M., Green S., 1994, MOLSCAT Computer Code (Ver. 14), Collaborative Computational Project No. 6. Engin. & Phys. Sci. Res. Counc., Swindon, UK
Jankowski P., Szalewicz K., 2005, J. Chem. Phys., 123, 104301
Jeziorska M., Jankowski P., Szalewicz K., Jeziorski B., 2000, J. Chem. Phys., 113, 2957
Kawaguchi K., Kasai Y., Ishikawa S.-I., Ohishi M., Kaifu N., Amano T., 1994, ApJ, 420, L95
Knizia G., Adler T. B., Werner H.-J., 2009, J. Chem. Phys., 130, 054104
Knowles Peter J., Werner H.-J., 1985, Chem. Phys. Lett., 115, 259
Kołos R., Grabowski Z. R., 2000, Ap&SS, 271, 65
Kunde V., Aikin A., Hanel R., Jennings D., Maguire W., Samuelson R., 1981, Nature, 292, 686
Manolopoulos D., 1986, J. Chem. Phys., 85, 6425
McLain J., Adams N., 2009, Planet. Space Sci., 57, 1642
Milligan D., Fairley D., 1998, Int. J. Mass Spectrom, 179, 180
Nkem C., Hammami K., Halalaw I. Y., Owono L. C. O., Jaidane N.-E., 2014, Ap&SS, 349, 171
North S. W., Hall G. E., 1997, J. Chem. Phys., 106, 60
Petrie S., Millar T., Markwick A., 2003, MNRAS, 341, 609
Puzzarini C., Cazzoli G., 2009, J. Mol. Spectrosc., 256, 53
Riechers D. A., Walter F., Cox P., Carilli C. L., Weiss A., Bertoldi F., Neri R., 2007, ApJ, 666, 778
Rodriguez-Franco A., Martin-Pintado J., Fuente A., 1998, A&A, 329, 1097
Roueff E., Lique F., 2013, Chem. Rev., 113, 8906
Semaniak J. et al., 2001, ApJS, 135, 275
Werfelli G., Balança C., Stoecklin T., Kerkeni B., Feautrier N., 2017, MNRAS, 468, 2582
Werner H.-J., Knowles Peter J., 1985, J. Chem. Phys., 82, 5053
Werner H.-J. et al., 2010, http://www. molpro.net
Wernli M., Wiesenfeld L., Faure A., Valiron P., 2007, A&A, 464, 1147
Wu M., Hall G. E., 1994, J. Photochem. Photobiol. A: Chem., 80, 45
Ziurys L., Apponi A., Yoder J., 1992, ApJ, 397, L123

SUPPORTING INFORMATION

Supplementary data are available at *MNRAS* online.

sup-mat.pdf

Please note: Oxford University Press is not responsible for the content or functionality of any supporting materials supplied by the authors. Any queries (other than missing material) should be directed to the corresponding author for the article.

This paper has been typeset from a TEX/LATEX file prepared by the author.